Stress analysis in cylindrical composition-gradient electrodes of lithium-ion battery

Yaotian Zhong, Yulan Liu, and B. Wang

Citation: AIP Advances **7**, 075115 (2017); doi: 10.1063/1.4986542
View online: https://doi.org/10.1063/1.4986542
View Table of Contents: http://aip.scitation.org/toc/adv/7/7
Published by the American Institute of Physics

Stress analysis in cylindrical composition-gradient electrodes of lithium-ion battery

Yaotian Zhong, Yulan Liu,[a] and B. Wang[b]
School of Engineering, Sun Yat-Sen University, Guangzhou 510275, China and
School of Physics, Sun Yat-Sen University, Guangzhou 510275, China

(Received 31 March 2017; accepted 17 July 2017; published online 26 July 2017)

In recent years, the composition-gradient electrode material has been verified to be one of the most promising materials in lithium-ion battery. To investigate diffusion-induced stresses (DIS) generated in a cylindrical composition-gradient electrode, the finite deformation theory and the stress-induced diffusion hypothesis are adopted to establish the constitutive equations. Compared with stress distributions in a homogeneous electrode, the increasing forms of Young's modulus E(R) and partial molar volume Ω(R) from the electrode center to the surface along the radial direction drastically increase the maximal magnitudes of hoop and axial stresses, while both of the decreasing forms are able to make the stress fields smaller and flatter. Also, it is found that the slope of -1 for E(R) with that of -0.5 for Ω(R) is a preferable strategy to prevent the inhomogeneous electrode from cracking, while for the sake of protecting the electrode from compression failure, the optimal slope for inhomogeneous E(R) and the preferential one for Ω(R) are both -0.5. The results provide a theoretical guidance for the design of composition-gradient electrode materials. [http://dx.doi.org/10.1063/1.4986542]

I. INTRODUCTION

As one of the most promising secondary cells, the lithium-ion battery has been the stored-energy apparatus of many portable electronic devices and transportations due to its high energy density, long cycle life, high open-circuit voltage, low self-discharge rate and its environmental friendly merit. However, shortcomings of lithium-ion batteries, such as high cost and low energy storage capacity, restrict its applications in hybrid electric vehicles and electric vehicles. Therefore, lowering the manufacturing costs and enlarging the energy storage capacity become a strategic goal of breaking LIBs' bottleneck of application.[1,2] Although based on the current research, as anode materials, silicon has the highest lithium-ion intercalation capacity (4200mAh/g) which is ten times of that in graphite materials commonly used in commerce.[3,4] When a silicon anode absorbs or desorbs lithium, it will generate about 300 to 400 percent of volume deformation in the electrode. After the first charged-discharged cycling, large stresses leads the silicon electrode to crack or degrade electrochemically.[5–7] As cathode materials commonly used at present, $LiCoO_2$ suffers from its toxicity on the human body and high cost due to limited sources of cobalt ore.[1,8] Moreover, the stresses produced by deformation of $LiCoO_2$ cathodes may cause the electrode to fracture when it is constrained.[9] So searching for the substitution and improving the preparation technology have become a hotspot in LIB anode materials. Among advanced materials substituted for $LiCoO_2$, composition-gradient materials shows better electrochemical performances, such as thermostability and its excellent cycle performance.[10,11] Even though the study of composition-gradient materials just focuses on simple shapes like sphere. It is believed that there will be different shapes

[a]E-mail: stslyl@mail.sysu.edu.cn
[b]E-mail: wangbiao@mail.sysu.edu.cn

of composition-gradient electrodes synthesized as technologies of synthesis process are improved. Hence, it is of major importance for us to study the electrochemical and mechanical properties of composition-gradient electrodes in different shapes. With the analysis of DIS affected by these properties, it provides a theoretical strategy to guide the design of composition-gradient electrode materials.

The initial research of diffusion-induced stresses (DIS) in silicon wafer were started by Prussin.[12] From then on, the study of DIS in various compositional and structural solids attracts many attention of researchers. Li[13] studied DISs generated in solid ferrite doped with excess nitrogen in different simple shapes such as thin plates, cylinders and spheres. Recently Yang et al.[14] analyzed the stresses caused by insertion deformation within a spherical electrode particle in potentiostatic and galvanostatic conditions. Song et al.[15] and Li et al.[16] computed the analytical expressions of DISs in cylindrical electrode, while Zhang et al.[17] introduced Young's modulus ratio and axial lithiation expansion coefficient ratio to isotropic case to investigate stresses generated in transversely isotropic cylindrical electrodes of lithium-ion batteries. Yang and Li[18] modelled a MEMS microcantilever sensor bending induced by dopant diffusion and evaluated DISs caused in beam structure. Zhang et al.[19] provided the formulas of stresses and compared solutions of reaction induced stress with that of diffusion induced stress during reversible electrochemical reaction in cylindrical Li-ion battery electrodes.

The studies above investigated DISs based on the linear elastic theory, neglecting nonlinear influence of large deformation. Besides, the literatures were established on the basis of the Fick's law, ignoring the interaction between diffusion and stresses. There are many achievements in these aspects. Hao and Fang[20,21] studied DISs of core-shell electrode by introducing a chemical potential coupling for diffusion and stresses. However, they still didn't consider the effect of large deformation. A large plastic deformation theory was formulated by Zhao and his co-workers[22] based on nonequilibrium thermodynamics. And they mainly analyzed the effect of plastic yielding on the magnitude of stress in the amorphous silicon electrode. Cui et al.[23] investigated the phase interface based on a model that accounts for the finite deformation kinematics and stress-diffusion interaction.

In this paper, a general framework to consider the mechanical behavior of a cylindrical composition-gradient electrode is formulated. Our theory incorporates the interaction of diffusion and stress as well as the finite deformation. Then we discussed a situation where the composition-gradient electrode is constrained in the axial direction. Furthermore, comparing the results of composition-gradient and homogeneous electrodes, we try to determine preferable inhomogeneous factors mechanically which may guide the design of composition-gradient electrodes.

There are two kind of new-style composition-gradient material synthesized as spherical electrode particle, one of which is $LiMn_{1.87}Ni_{0.13}O_4$ and the other is $Li_{1.2}(Mn_{0.62}Ni_{0.38})_{0.8}O_2$.[24,25] The former has a concentration-gradient shell region where the concentration of Ni increases and that of Mn decreases from the core to its surface while the latter has an opposite trend in the concentration-gradient shell region. Both of them have excellent characteristics in the electrochemical performance. The thermostable composition-gradient electrode $LiMn_{1.87}Ni_{0.13}O_4$ shows its superior cyclability with a capacity retention of 90. 2% after 200 cycles at 55°C, while the $LiMn_2O_4$ in the same test conditions exhibited only 57. 8%. And the novel composition-gradient electrode $Li_{1.2}(Mn_{0.62}Ni_{0.38})_{0.8}O_2$ retained 97% of its capacity after 100 cycles relative to the first cycle at a rate of C/2. However, there is few of literatures focusing on the mechanical and electrochemical properties about these new material. So we try to adopt the mechanical and electrochemical parameters of $LiMn_2O_4$ to study the mechanical difference between composition-gradient electrodes and homogeneous electrodes indirectly. Namely, it is assumed that the mechanical and electrochemical properties change continuously from electrode center to its surface. Also, the effect of plasticity in a composition-gradient electrode is ignored since there are no obvious plastic deformation in these lithium nickel manganese oxide material.[24,26] Besides, it is assumed that the effect of concentration-dependence of Young's modulus is not discussed in our models.[27] Because it may play a small role in stresses generated in concentration-gradient electrode materials.

II. BASIC THEORY

A. Mechanical equilibrium

When lithium-ions diffuse into or out of the electrode, large volume deformation may be generated in the electrode. There are two descriptions which are Lagrangian form and Eulerian form. The former is based on the initial configuration, while the latter is based on the current configuration. In the cylindrical coordinate, a point of the electrode at (R, Θ, Z) in the Lagrangian description moves to (r, θ, z) in the Eulerian description after a period of time t. So the total deformation gradient tensor in the cylindrical coordinate is defined as

$$\mathbf{F} = \langle F_{11}, F_{22}, F_{33} \rangle = \left\langle 1 + \frac{\partial u}{\partial R}, 1 + \frac{u}{R}, 1 + \frac{\partial w}{\partial Z} \right\rangle, \tag{1}$$

where u is the radial displacement, and w is the axial displacement. The total deformation $\mathbf{F}$ can be decomposed into elastic part $\mathbf{F}^{\mathrm{e}}$ and inelastic part $\mathbf{F}^{\mathrm{i}}$ without consideration of the plasticity of the composition-gradient electrode.

$$\mathbf{F} = \mathbf{F}^e \mathbf{F}^i, \tag{2}$$

An isotropic form of inelastic deformation gradient tensor is adopted as follow.[28]

$$\mathbf{F}^i = \left(\Lambda^i\right)^{\frac{1}{3}} \mathbf{I}, \tag{3}$$

where $\mathbf{I}$ is the unit tensor and Λ^{i} is the inelastic volume ratio since the inelastic deformation depends on the volume change caused by lithium-ions diffusion. So it is dominated by the lithium-ion concentration C based on the Lagrangian description. With the diffusion partial molar volume Ω, the inelastic volume ratio is expressed as

$$\Lambda^i = 1 + \Omega C, \tag{4}$$

And the components of the elastic deformation gradient tensor $\mathbf{F}^{\mathrm{e}}$ is given as

$$\mathbf{F}^e = \mathbf{F}\left(\mathbf{F}^i\right)^{-1} = \left\langle \left(1 + \frac{\partial u}{\partial R}\right)\left(\Lambda^i\right)^{-\frac{1}{3}}, \left(1 + \frac{u}{R}\right)\left(\Lambda^i\right)^{-\frac{1}{3}}, \left(1 + \frac{\partial w}{\partial Z}\right)\left(\Lambda^i\right)^{-\frac{1}{3}} \right\rangle, \tag{5}$$

According to the assumption above, the material properties change along the radial direction, while it remain the same along the azimuthal and the axial direction in a cylindrical composition-gradient electrode. Therefore, the partial molar volume Ω, the elasticity modulus E and the diffusion coefficient D are functions of radial coordinate in the Lagrangian description. It follows from Eq. (2) that the total Green-Lagrange strain tensor $\mathbf{E}$, the elastic Green-Lagrange strain tensor $\mathbf{E}^{\mathrm{e}}$ and the inelastic Green-Lagrange strain tensor $\mathbf{E}^{\mathrm{i}}$ can be written as

$$\mathbf{E} = \frac{1}{2}\left(\mathbf{F}^T\mathbf{F} - \mathbf{I}\right), \tag{6}$$

$$\mathbf{E}^e = \frac{1}{2}\left(\left(\mathbf{F}^e\right)^T\mathbf{F}^e - \mathbf{I}\right), \tag{7}$$

$$\mathbf{E}^i = \frac{1}{2}\left(\left(\mathbf{F}^i\right)^T\mathbf{F}^i - \mathbf{I}\right), \tag{8}$$

where $\mathbf{I}$ is the second order unit matrix.

Here, we use an elastic strain energy density in the Lagrangian description as follow[23,29]

$$W = \Lambda^i \frac{E}{2(1+\upsilon)}\left\{\frac{\upsilon}{1-2\upsilon}\left[tr\left(\mathbf{E}^e\right)\right]^2 + tr\left(\mathbf{E}^e\mathbf{E}^e\right)\right\}, \tag{9}$$

E and υ are the Young's modulus and Poisson's ratio of the composition-gradient electrode, respectively. Moreover, the non-zero components of the first Piola-Kirchhoff stress $\boldsymbol{\sigma}^0$ can be determined by

$$\boldsymbol{\sigma}^0 = \frac{\partial W}{\partial \mathbf{F}} = \frac{\partial W}{\partial \mathbf{E}^e}\frac{\partial \mathbf{E}^e}{\partial \mathbf{F}^e}\frac{\partial \mathbf{F}^e}{\partial \mathbf{F}}, \tag{10}$$

Substituting Eqs. (4) and (9) into Eq. (10), we can obtain

$$\boldsymbol{\sigma}^0 = \Lambda^i \frac{E}{2(1+\upsilon)} \left[\frac{2\upsilon}{1-2\upsilon} tr\left(\mathbf{E}^e\right) + 2\mathbf{E}^e \right] \frac{\mathbf{F}^e}{\mathbf{F}^i}, \tag{11}$$

Combining Eqs. (1), (3), (4), (5) and (7) with Eq. (11) leads to

$$\sigma_R^0 = (1+\Omega C) \frac{E}{(1+\upsilon)(1-2\upsilon)} \left[(1-\upsilon) E_R^e + v \left(E_\Theta^e + E_Z^e \right) \right] \frac{2E_R^e + 1}{1 + \dfrac{\partial u}{\partial R}}, \tag{12}$$

$$\sigma_\Theta^0 = (1+\Omega C) \frac{E}{(1+\upsilon)(1-2\upsilon)} \left[(1-\upsilon) E_\Theta^e + v \left(E_R^e + E_Z^e \right) \right] \frac{2E_\Theta^e + 1}{1 + \dfrac{u}{R}}, \tag{13}$$

$$\sigma_Z^0 = (1+\Omega C) \frac{E}{(1+\upsilon)(1-2\upsilon)} \left[(1-\upsilon) E_Z^e + v \left(E_\Theta^e + E_R^e \right) \right] \frac{2E_Z^e + 1}{1 + \dfrac{\partial w}{\partial Z}}, \tag{14}$$

where σ_R^0, σ_Θ^0 and σ_Z^0 are components of the first Piola-Kirchhoff stress $\boldsymbol{\sigma}^0$. E_R^e, E_Θ^e and E_Z^e are components of the elastic Green-Lagrange strain tensor $\mathbf{E}^e$ given as

$$E_R^e = \frac{1}{2} \left[\frac{\left(1 + \dfrac{\partial u}{\partial R}\right)^2}{(1+\Omega C)^{\frac{2}{3}}} - 1 \right], \tag{15}$$

$$E_\Theta^e = \frac{1}{2} \left[\frac{\left(1 + \dfrac{u}{R}\right)^2}{(1+\Omega C)^{\frac{2}{3}}} - 1 \right], \tag{16}$$

$$E_Z^e = \frac{1}{2} \left[\frac{\left(1 + \dfrac{\partial w}{\partial Z}\right)^2}{(1+\Omega C)^{\frac{2}{3}}} - 1 \right], \tag{17}$$

Here, the quasi-static mechanical equilibrium is assumed due to the much slower velocity of atomic diffusion over that of elastic deformation.[17] Then, the equations of mechanical equilibrium in the cylindrical coordinate are reduced as

$$\frac{\partial \sigma_R^0}{\partial R} + \frac{\sigma_R^0 - \sigma_\theta^0}{R} = 0, \tag{18}$$

$$\frac{\partial \sigma_Z^0}{\partial Z} = 0. \tag{19}$$

The mechanical equilibrium behavior is governed by Eqs. (12)~(19).

B. Diffusion equation

The diffusion kinetic equation in the Lagrangian description is expressed as follow based on the law of mass conservation[30]

$$\frac{\partial C}{\partial t} + \frac{\partial (RJ)}{R \partial R} = 0, \tag{20}$$

where C is the concentration of lithium-ions based on the Lagrangian description. J is defined as the radial diffusion flux of the solute in the Lagrangian description. And the true concentration of lithium-ions c can be determined by C as follow

$$C = c \cdot det\,(\mathbf{F}) = c F_R F_\Theta F_Z, \tag{21}$$

where F_R, F_Θ and F_Z are components of the total deformation gradient tensor $\mathbf{F}$.

The true diffusion flux j is a function of the chemical potential μ.

$$j = -\frac{cD}{R_g T}\frac{\partial \mu(r,c)}{\partial r}, \tag{22}$$

where D is the diffusivity of Lithium-ions in the electrode, R_g is the universal gas constant and T is the temperature. Combining Eqs. (21) with (22), the diffusion flux J can be deduced as

$$J = -\frac{CD}{R_g T}\frac{1}{F_R^2}\frac{\partial \mu(R,C)}{\partial R}, \tag{23}$$

where μ(R, C) is expressed by the Lagrangian coordinates.

Here, the form of the chemical potential is adopted as[22]

$$\mu(r,c) = \mu_0 + R_g T log(\gamma c) - \Omega\sigma_m, \tag{24}$$

where μ(r, c) is the chemical potential based on the Euler description, μ_0 is a reference value, γ is the activity coefficient and σ_m is the hydrostatic stress. We let γ equal to 1.

From Eqs. (21)~(23), we can obtain

$$J = jF_\Theta F_Z, \tag{25}$$

Substituting Eq. (24) into Eq. (22) and combining Eq. (25), the diffusion flux J is formulated as

$$J = -D\frac{F_\Theta F_Z}{F_R}\frac{\partial}{\partial R}\left(\frac{C}{F_R F_\Theta F_Z}\right) + \frac{1}{R_g T}\frac{CD}{F_R^2}\left(\frac{\partial \Omega}{\partial R}\sigma_m + \frac{\partial \sigma_m}{\partial R}\Omega\right), \tag{26}$$

where the diffusion partial molar volume Ω is a function of the radial coordinate R in the Lagrangian description. And the hydrostatic stress σ_m is expressed as

$$\sigma_m = \frac{1}{3}(\sigma_R + \sigma_\Theta + \sigma_Z), \tag{27}$$

while the first Piola-Kirchhoff stress $\boldsymbol{\sigma}^0$ and the Cauchy stress $\boldsymbol{\sigma}$ have a relationship as follow

$$\boldsymbol{\sigma}^0 = det(\mathbf{F})\boldsymbol{f}\boldsymbol{\sigma}, \tag{28}$$

in which $\boldsymbol{f} = \frac{\partial \mathbf{X}}{\partial \mathbf{x}} = \mathbf{I} - \frac{\partial \mathbf{u}}{\partial \mathbf{x}}$.

Therefore, the Cauchy stress $\boldsymbol{\sigma}$ can be denoted by the first Piola-Kirchhoff stress $\boldsymbol{\sigma}^0$ as

$$\boldsymbol{\sigma} = \langle \sigma_R, \sigma_\Theta, \sigma_Z \rangle = \left\langle \frac{1}{\left(1+\frac{u}{R}\right)\left(1+\frac{\partial w}{\partial Z}\right)}\sigma_R^0, \frac{1}{\left(1+\frac{\partial u}{\partial R}\right)\left(1+\frac{\partial w}{\partial Z}\right)}\sigma_\Theta^0, \frac{1}{\left(1+\frac{\partial u}{\partial R}\right)\left(1+\frac{u}{R}\right)}\sigma_Z^0 \right\rangle. \tag{29}$$

The diffusion kinetic behavior is dominated by Eqs. (20), (26) and (29).

C. Boundary and initial conditions

We assume that the radial surface of the cylinder is stress-free and the cylindrical center has no displacement, that is

$$\sigma_R^0(R_0, t) = 0, \tag{30}$$

$$u(0, t) = 0, \tag{31}$$

Besides, potentiostatic operation is set at the surface of the cylinder resulting in a constant concentration C_{max} there, that is

$$C(R_0, t) = C_{max}, \tag{32}$$

while the boundary conditions substituting for Eq. (32) are given by

$$J(R_0, t) = \frac{i_n}{F}, \tag{33}$$

corresponding to the galvanostatic discharging process. Meanwhile, i_n is the applied current density and F is the Faraday's constant.

At the center of the cylinder, the diffusion flux J is given as

$$J(0,t)=0, \tag{34}$$

Physical constraints are imposed on the top and bottom faces of the cylinder in order to constrain the deformation of the ends in the axial direction. We hypothesize that such constraints may not prevent the ends of the cylinder from moving in the lateral direction, that is w=0 on the faces of the ends.

At last, we adopt Li-free, stress-free and displacement-free initial conditions in the cylinder, that is

$$C(R,0)=0, \tag{35}$$

$$u(R,0)=0, \tag{36}$$

III. RESULTS AND DISCUSSION

Since there is bare possibility of getting the analytical solution of equations above, we solve numerically the system of equations described in Section II by using the finite element method (COMSOL Multiphysics). Also, it is difficult to obtain the mechanical and electrochemical properties of the composition-gradient electrodes $LiMn_{1.87}Ni_{0.13}O_4$ or $Li_{1.2}(Mn_{0.62}Ni_{0.38})_{0.8}O_2$. The exact functions of E(R) and Ω(R) have not been fully understood and studied. Following the previous assumption,[28] these functions are linear with several different slopes of radial coordinate R. Once the properties are constant along the radial coordinate, the inhomogeneous theory in Section II reduces to the theory in a homogeneous cylindrical particle of $LiMn_2O_4$. The main purpose for this paper is to study different gradient effect of properties on DISs in a cylindrical composition-gradient electrode during potentiostatic charging and galvanostatic discharging. To achieve this goal, we divide this section into two parts. Following the previous method,[32] in the first part, we discuss DISs initially from two specific conditions. In the first condition, inhomogeneous properties increase respectively from the center to the surface with the slope of 1, while the second is the decreasing form with the slope of -1. And we study the gradient effect of properties with different slopes on DISs at two specific positions where the maximal DISs happen in the second part. The material properties of $LiMn_2O_4$ are listed in Table I,[28] which will be also used as reference values in a cylindrical composition-gradient electrode. And the Faraday's constant is 96485.3365 A s mol^{-1}.[31] Here, it is defined that the increasing form means properties increase from the electrode center to the surface, while the decreasing form means the opposite situation. And the normalized time τ is represented as

$$\tau = Dt/R_0^2, \text{ where t is the real time.} \tag{37}$$

Here, the state of charging (SOC), is used to represent the percentage of full capacity and to evaluate the charging process of the cylinder. Thus, SOC is given as[33]

TABLE I. Material properties and operating parameters of $LiMn_2O_4$.[28]

Parameter	Symbol	Value
Young's modulus	E_0	10 GPa
Poisson's ratio	υ	0. 3
Surface lithium-ion concentration	C_{max}	2. 29×10^4 $mol\ m^{-3}$
Diffusion partial molar volume	Ω_0	3. 497×10^{-6} $m^3\ mol^{-1}$
Gas constant	R_g	8. 31 J $mol^{-1}\ K^{-1}$
Diffusion coefficient	D_0	7. 08×10^{-15} $m^2\ s^{-1}$
Temperature	T	273 K
Faraday's constant	F	96485.3365 $A\ s\ mol^{-1}$[31]
Current density	i_n	2.0 A m^{-2}[31]
Cylinder radius	R_0	2×10^{-7} m

$$SOC = \frac{\int_0^{R_0} CR^2 dR}{\int_0^{R_0} C_{steady-state} R^2 dR}, \tag{38}$$

It is assumed that E(R) and Ω(R) are simple linear functions of R given as follow

$$E(R) = a_1\left(R - \frac{R_0}{2}\right) + E_0, \Omega(R) = a_2\left(R - \frac{R_0}{2}\right) + \Omega_0 \tag{39}$$

where a_1 and a_2 are respectively slopes of properties. E_0 and Ω_0 are properties of homogeneous $LiMn_2O_4$ material. Namely, the properties at 1/2 radius R_0 are defined the same as those of $LiMn_2O_4$ material. Then k_1 and k_2 are normalized as

$$k_1 = \frac{R_0}{E_0} a_1, k_2 = \frac{R_0}{\Omega_0} a_2. \tag{40}$$

where k_1 and k_2 are respectively dimensionless slopes of the Young's modulus and partial molar volume.

A. Two specific conditions

The results of a homogeneous cylindrical particle are plotted by solid lines, while the results of an inhomogeneous cylindrical particle are plotted by dashed lines. And If not state particularly, all results in this part follow this rule.

According to the previous research,[28] inhomogeneous diffusion coefficient D(R) only influences the velocity of diffusion. Nevertheless, there is little difference on stresses between homogeneous and inhomogeneous D(R) materials. Thus, the effect of inhomogeneous D(R) on Li-ions diffusion is not discussed here. It is noted that E on illustrations below means the Young's modulus value of homogeneous $LiMn_2O_4$ materials.

Fig. 1 and Fig. 2 illustrate the stress fields for homogeneous and inhomogeneous elastic modulus E(R) at different normalized time. Figures of the lithium-ion concentration distributions are not

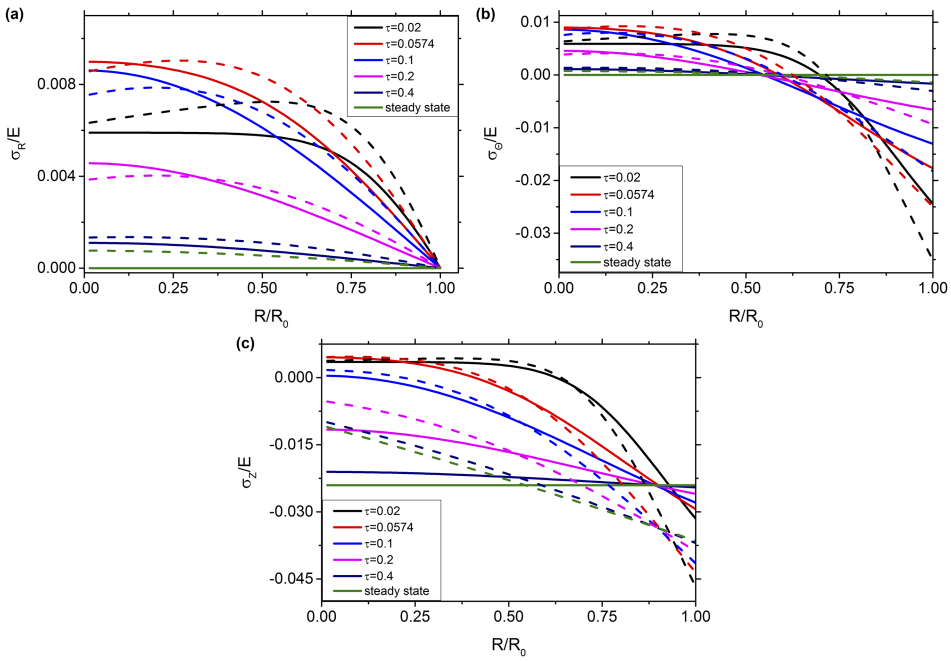

FIG. 1. Illustrations of radial stress (a), hoop stress (b) and axial stress (c) of homogeneous and inhomogeneous elastic modulus E(R) at different normalized time.

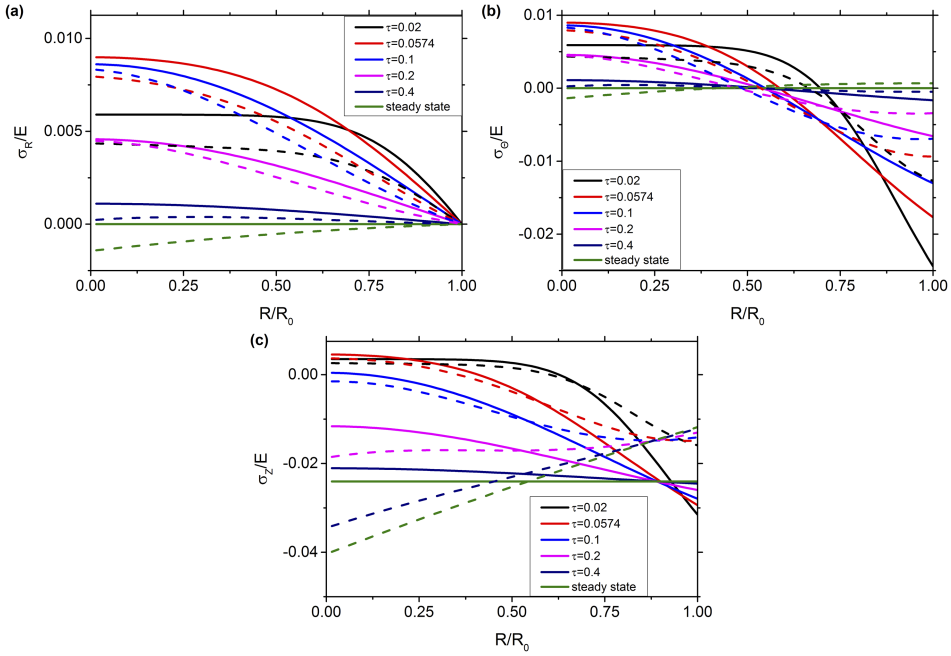

FIG. 2. Illustrations of the stress fields of homogeneous and inhomogeneous elastic modulus E(R) at different normalized time.

exhibited here since inhomogeneous E(R) has little influence on lithium-ion distribution comparing with that in a homogeneous electrode. Comparing Fig. 1(b) with Fig. 2(b), at the electrode surface, we know that positive gradient E(R) drastically increases the value of hoop stresses, while negative gradient E(R) can effectively decrease the magnitudes of hoop stresses. In Fig. 1(c) and Fig. 2(c), at the electrode center, inhomogeneous E(R) hardly affects the axial stress values in the beginning and make a great difference later that positive gradient E(R) reduces the magnitudes of axial stresses and negative gradient E(R) leads to the opposite result. By contrast, at the electrode surface, negative gradient E(R) sharply decreases the magnitudes of axial stresses, while it leads to the opposite result in an inhomogeneous electrode of positive gradient E(R). And it should be noted that the stress distributions, especially the axial stress, change unevenly along the coordinate R at the steady state, while the stress distributions are flat in a homogeneous electrode.

Fig. 3 and Fig. 4 illustrate the concentration and stress fields of homogeneous and two specific inhomogeneous partial molar volume Ω(R) at different normalized time. Comparing dashed lines with solid lines in Fig. 3(a) and Fig. 4(a), inhomogeneous Ω(R) nearly has no influence on concentration distributions at the beginning. As the charging process is going ahead, the positive gradient Ω(R) accelerates the diffusion process later, while negative gradient Ω(R) shows the opposite result.

At the electrode center, we can find in Fig. 3(b, c, d) that positive gradient Ω(R) obviously increases the values of tensile stresses and greatly increases the magnitudes of hoop stresses and axial stresses at the electrode surface. Also, at the electrode surface, the maximal magnitudes of the hoop stress and the axial stress in a positive gradient Ω(R) electrode are respectively the same as those in a positive gradient E(R) electrode at the slope of 1. So it is easy for us to wonder if the maximal stress values for inhomogeneous Ω(R) are the same respectively at different slopes comparing with that for inhomogeneous E(R). This issue will be discussed in Section III B. In Fig. 4(b, c, d), at the electrode center, we know that negative gradient Ω(R) greatly increases the magnitudes of compressive stresses at the steady state but effectively decreases the values of tensile stresses, while at the electrode surface, negative gradient Ω(R) effectively decreases the values of compressive hoop and axial stresses but the hoop stress turns to tensile at the steady state. The results are quite different from that in plane stain method.[34] Although stress distributions become flatter than that in a homogeneous electrode, tensile hoop stresses in the surface may lead to mechanical fracture of the negative gradient Ω(R) electrode.

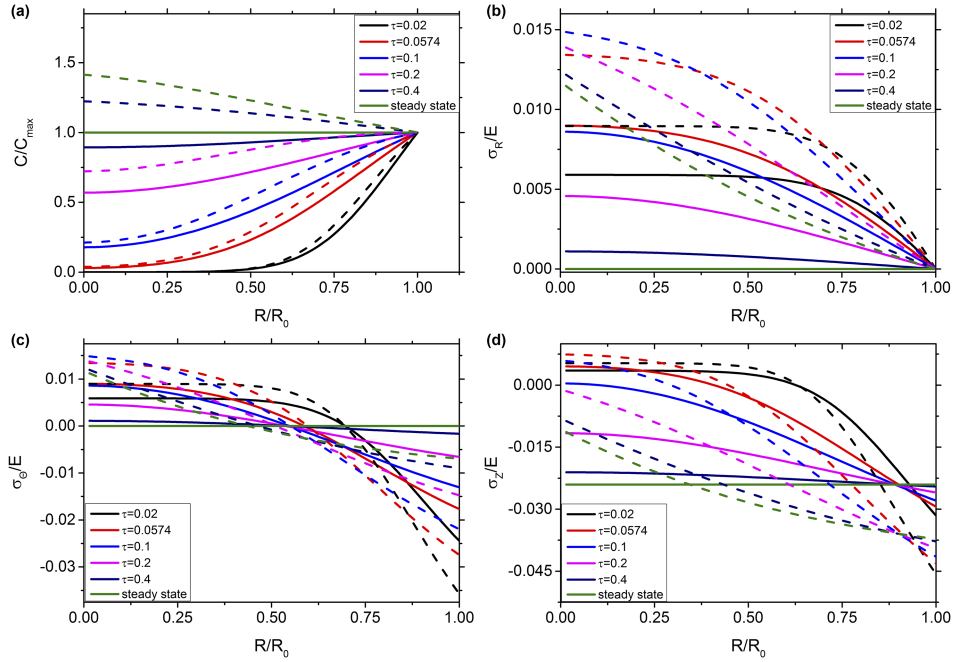

FIG. 3. Illustrations of lithium-ion concentration (a), radial stress (b), hoop stress (c) and axial stress (d) of homogeneous and inhomogeneous partial molar volume Ω(R) at different normalized time.

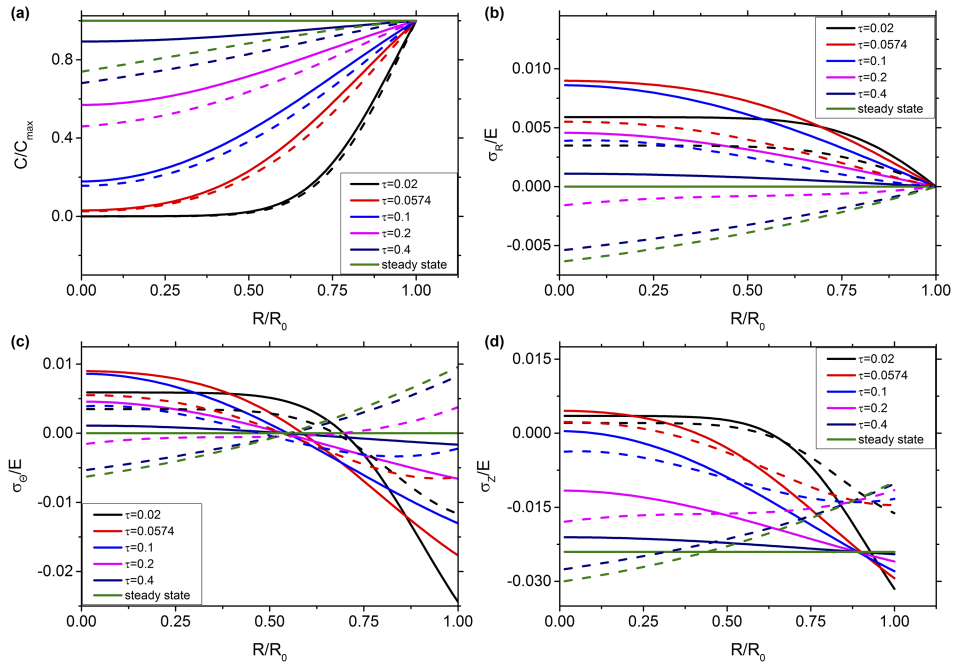

FIG. 4. Illustrations of the concentration distribution and stress fields of homogeneous and inhomogeneous partial molar volume Ω(R) at different normalized time.

B. Two inhomogeneous factors in different slopes k

From Section III A, we have already known that the maximal compressive stresses happen at the beginning of diffusion at the electrode surface during potentiostatic charging while the maximal tensile stresses are generated at the center. Secondly, it is noticed that at the steady state, stress fields in

an inhomogeneous electrode, especially for inhomogeneous E(R) and Ω(R), are significantly different from that in a homogeneous electrode. To further study the effect of inhomogeneous E(R) and Ω(R) on stress distributions at the positions mentioned above, we choice two critical positions, the center and the surface of electrodes where the maximal stresses are possibly generated. And our purpose is to find and evaluate the optimal slope of E(R) and Ω(R) to reduce the maximal stresses.

In Section III B, we also calculate DISs in the heterogeneous E(R) and Ω(R) electrode during galvanostatic discharging. Firstly, the heterogeneous E(R) and Ω(R) models with different slopes k are charged to SOC=90% in a constant voltage. Next, we will make them respectively discharged in a constant current density i_n. The results of the center and surface are discussed in this section. And it should be noted that the positive slope k means inhomogeneous factors increase from the electrode center to its surface, while the negative k represents the opposite situation.

The result shows that radial stresses are equal to hoop stresses at electrode center at the same normalized time. Moreover, radial stresses are defined as zero at the cylindrical surface in the boundary condition. Thus, they are no need discussed here.

The explanation is made to describe illustrations in Section III B before discussion. Panels (a, b) represent the results at the center of the electrode, while panels (c, d) represent that at the surface. Besides, illustrations (a, c) correspond to the result in potentiostatic charging condition, while illustrations (b, d) correspond to that in galvanostatic discharging condition. If there is no special statement, all graphs in Section III B follow this regulation.

Fig. 5 illustrates hoop stresses at different slopes of inhomogeneous E(R) at the center and surface of an electrode. From Fig. 5(a, b), we can find that the maximal positive hoop stress reaches as high as 0.008~0.009 during constant-voltage charging process. It is much larger than that in Fig. 5(b) during the discharging process. So, there is a proper way for us to discuss the effect of different slopes of E(R) on hoop stresses in Fig. 5(a) rather than Fig. 5(b). And it can be concluded that inhomogeneous E(R) is able to decrease the maximal value of tensile hoop stress. We also infer from Fig. 5(a) that the larger absolute value of the slope k, the smaller maximum tensile hoop stress it is. In addition, it is found in Fig. 5(b) that as the galvanostatic discharging process becomes steady, only the hoop stress of homogeneous material is convergent to zero while the results of increasing forms of E(R) approach tension and those of decreasing forms of E(R) approach compressive stress.

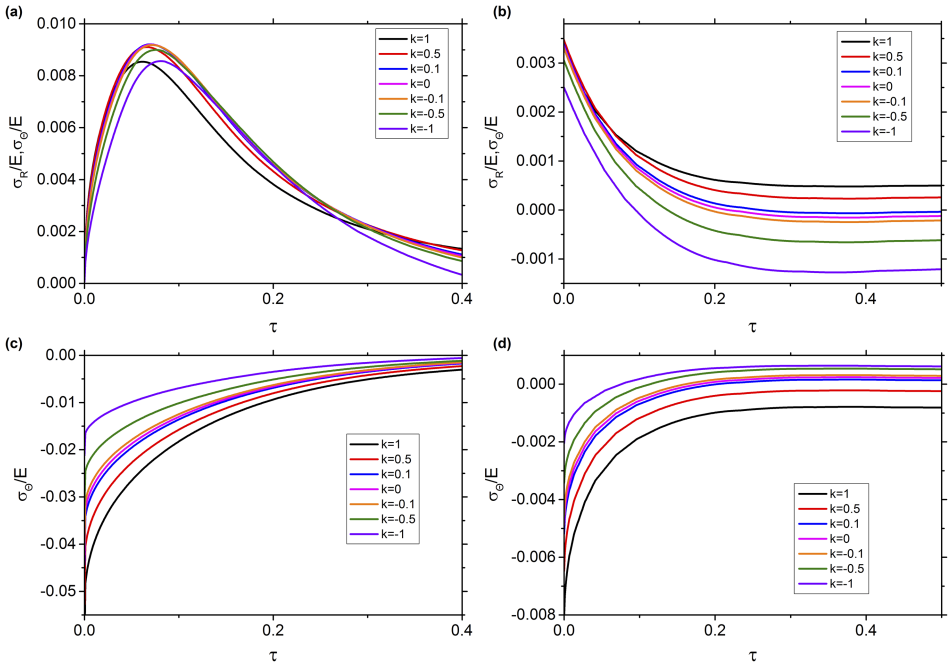

FIG. 5. Illustrations of radial or hoop stress (a, b) and hoop stress (c, d) of the inhomogeneous elastic modulus E(R) in different slopes k.

On the contrary in Fig. 5(d), the hoop stress of a decreasing form of E(R) is convergent to a tensile value, while that of an increasing form approaches a compressive value at the surface of the electrode at the discharging steady state. It is obviously that decreasing forms of E(R) are able to decrease the hoop stress markedly at the electrode's surface upon the initial charging in Fig. 5(c).

As we all know that high tensile stresses easily generate cavities or void space,[22,35] resulting in a degradation of electrodes and the decline of their cycling performance. To prevent the risk, the slope of -1 is probably the optimal slope for an inhomogeneous E(R) electrode because it decreases the maximal tensile stress at the center and also tremendously reduces the maximal stress at the surface.

The variation of axial stresses with the normalized time τ are displayed in Fig. 6. It is obvious that the electrode is mainly under pressure in the axial direction. Unlike Fig. 5, the magnitude of axial stresses among graphs in Fig. 6 are in the same order. Therefore, we need to analyze and evaluate the axial stresses in all four graphs. It is found that increasing forms of E(R) can decrease the maximal axial stress at the electrode center in Fig. 6(a), while they increase the result at the surface of the electrode in Fig. 6(c). Decreasing forms of E(R) show the opposite results. By contrast with maximum stresses in Fig. 6, it inspires us that the slope of -0.5 is probably the optimal slope for an inhomogeneous E(R) electrode because the maximal magnitude of axial stresses at the center is nearly equal to that at the surface.

It illustrates hoop stresses at different slopes of inhomogeneous Ω(R) at the center and surface of an electrode in Fig. 7. We can find that increasing forms of Ω(R) are able to increase the maximal tensile hoop stress at the center in Fig. 7(a), while decreasing forms of Ω(R) increase the tensile hoop stress at the electrode surface at the charging steady state in Fig. 7(c). Thus, on the analysis of the tensile stress in Fig. 7, the slope of -0.5 is more desirable than others for inhomogeneous Ω(R) due to the comparatively low tensile stress in the electrode. 0.0072 is the maximal magnitude of tensile normalized hoop stresses for the decreasing form of Ω(R) with the slope of -0.5 which is an advisable design to prevent an electrode from fracture and degradation.

Fig. 8 illustrates axial stresses at different slopes of inhomogeneous Ω(R) at the center and surface of an electrode. Similarly, increasing forms of Ω(R) decrease the maximal axial stress at the electrode center in Fig. 8(a), while they increase that at the surface of the electrode in Fig. 8(c). And decreasing forms of Ω(R) show the opposite result. Similar to Fig. 6, Fig. 8 shows

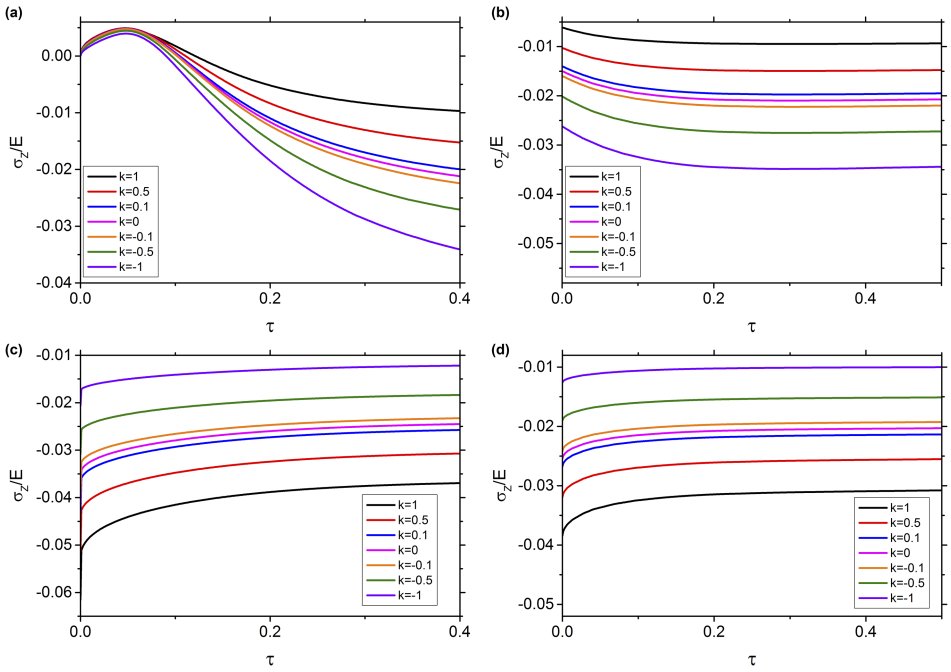

FIG. 6. Illustrations of axial stress during potentiostatic charging(a, c) and that during galvanostatic discharging(b, d) of the inhomogeneous elastic modulus E(R) in different slopes k.

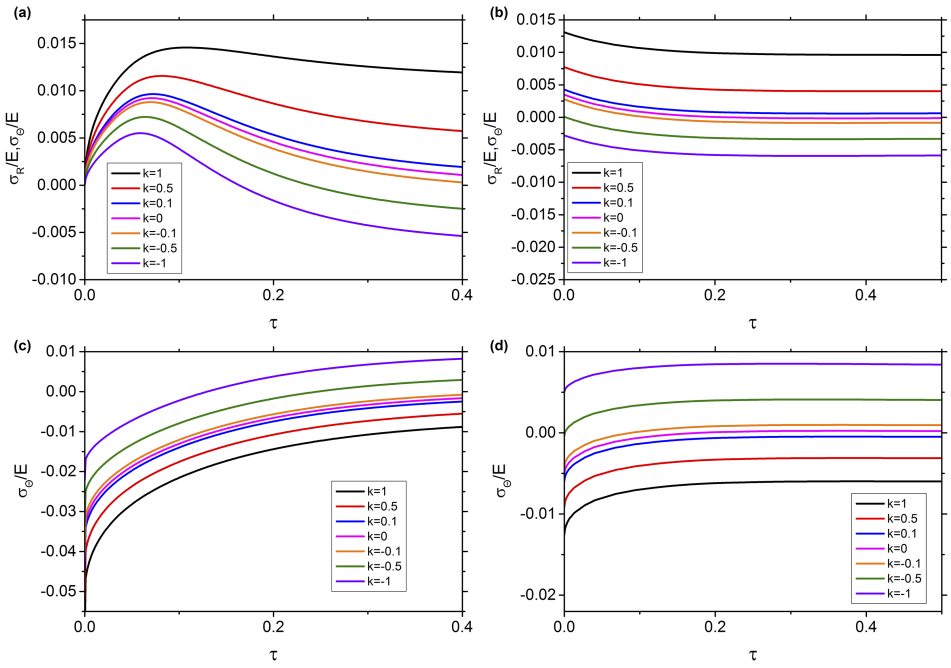

FIG. 7. Illustrations of radial or hoop stress (a, b) and hoop stress (c, d) of the inhomogeneous partial molar volume Ω(R) in different slopes k.

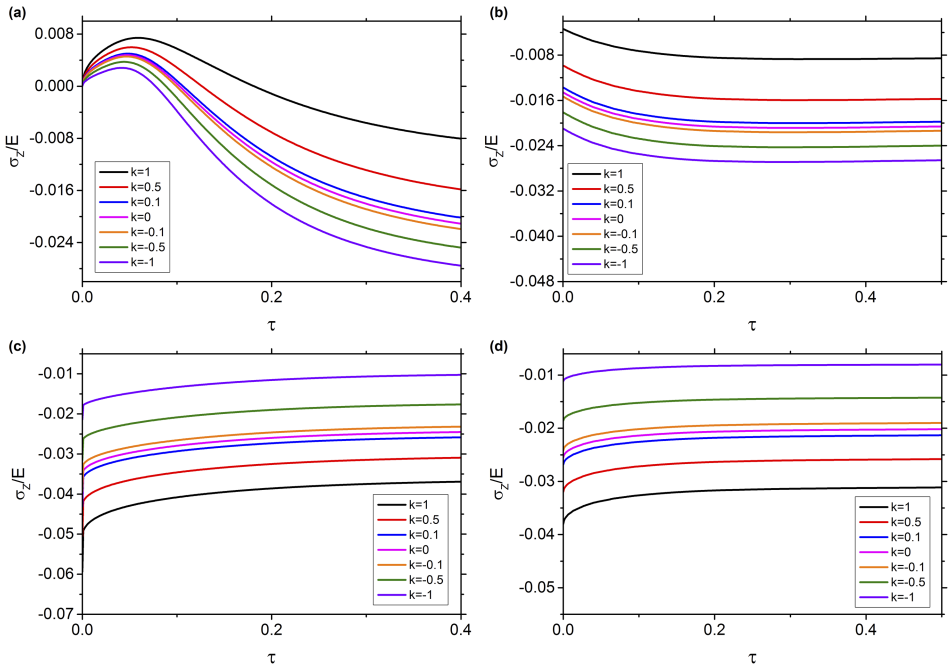

FIG. 8. Illustrations of axial stress during potentiostatic charging(a, c) and that during galvanostatic discharging(b, d) of the inhomogeneous partial molar volume Ω(R) in different slopes k.

that the choice of advisable Ω(R) slopes depends on the maximal axial stresses at the both positions of the electrode. For this reason, the slope of -0.5 is more preferable than others for inhomogeneous Ω(R) since it makes the same maximal axial stresses at both positions in charging and discharging conditions.

IV. CONCLUSION

We have formulated a theory in a cylindrical composition-gradient electrode constrained axially by considering the interaction effects of diffusion and stress in this paper. Combining with the diffusion theory and the finite deformation theory, the constitutive equations are established to analyze an electrode of being charged under potentiostatic operation and discharged under galvanostatic operation. Two inhomogeneous factors, Young's modulus E(R) and partial molar volume Ω(R) are respectively investigated. The increasing forms of E(R) and Ω(R) from the electrode center to its surface enlarge the maximum stresses comparing with that in a homogeneous electrode, while certain of decreasing forms of them are able to decrease the maximum stresses effectively and make stress distributions flatter. And we can find that the center and the surface of an electrode are two critical positions where the maximum stress are generated. Besides, we can conclude from Section III B that the slope of -1 for E(R) with that of -0.5 for Ω(R) is a preferable strategy to prevent an inhomogeneous electrode from fracture and degradation, while for the sake of protecting the electrode from compression failure, the optimal slope for inhomogeneous E(R) and the preferential one for Ω(R) are both -0.5. So the choice of the slope depends on the function and practical application of an electrode. These theoretical results need to be tested experimentally in future. And we hope that they provide some guidance on the design of composition-gradient electrodes.

ACKNOWLEDGMENTS

We are grateful for support from National Science Foundation under Grant No. 11572355 and Grant No. 10572155.

[1] J. M. Tarascon and M. Armand, Nature **414**, 359 (2001).
[2] M. Armand and J. M. Tarascon, Nature **451**, 652 (2008).
[3] U. Kasavajjula, C. Wang, and A. J. Appleby, Journal of Power Sources **163**, 1003 (2007).
[4] W.-J. Zhang, Journal of Power Sources **196**, 13 (2011).
[5] L. Y. Beaulieu, K. W. Eberman, R. L. Turner, L. J. Krause, and J. R. Dahn, Electrochemical and Solid-State Letters **4**, A137 (2001).
[6] X. Xiao, P. Liu, M. W. Verbrugge, H. Haftbaradaran, and H. Gao, Journal of Power Sources **196**, 1409 (2011).
[7] S. W. Lee, M. T. McDowell, L. A. Berla, W. D. Nix, and Y. Cui, Proceedings of the National Academy of Sciences of the United States of America **109**, 4080 (2012).
[8] J. B. Goodenough and Y. Kim, Chemistry of Materials **22**, 587 (2010).
[9] K. Zhao, M. Pharr, J. J. Vlassak, and Z. Suo, Journal of Applied Physics **108**, 073517 (2010).
[10] P. Y. Hou, L. Q. Zhang, and X. P. Gao, J. Mater. Chem. A **2**, 17130 (2014).
[11] W. Liu, P. Oh, X. Liu, M. J. Lee, W. Cho, S. Chae, Y. Kim, and J. Cho, Angew Chem Int Ed Engl **54**, 4440 (2015).
[12] S. Prussin, Journal of Applied Physics **32**, 1876 (1961).
[13] J. Chen-Min Li, Metallurgical Transactions A **9**, 1353 (1978).
[14] Y.-T. Cheng and M. W. Verbrugge, Journal of Power Sources **190**, 453 (2009).
[15] Y. Song, B. Lu, X. Ji, and J. Zhang, Journal of the Electrochemical Society **159**, A2060 (2012).
[16] J. Li, Q. Fang, F. Liu, and Y. Liu, Journal of Power Sources **272**, 121 (2014).
[17] X. y. Zhang, F. Hao, H. s. Chen, and D. n. Fang, Journal of the Electrochemical Society **161**, A2243 (2014).
[18] F. Yang and J. C. M. Li, Journal of Applied Physics **93**, 9304 (2003).
[19] T. Zhang, Z. Guo, Y. Wang, and J. Zhu, Journal of Applied Physics **115**, 083504 (2014).
[20] F. Hao and D. Fang, Journal of Applied Physics **113**, 013507 (2013).
[21] F. Hao and D. Fang, Journal of the Electrochemical Society **160**, A595 (2013).
[22] K. Zhao, M. Pharr, S. Cai, J. J. Vlassak, and Z. Suo, Journal of the American Ceramic Society **94**, s226 (2011).
[23] Z. Cui, F. Gao, and J. Qu, Journal of the Mechanics and Physics of Solids **61**, 293 (2013).
[24] Q. Wei, X. Wang, X. Yang, B. Ju, B. Hu, H. Shu, W. Wen, M. Zhou, Y. Song, H. Wu, and H. Hu, Journal of Materials Chemistry A **1**, 4010 (2013).
[25] G. M. Koenig, I. Belharouak, H. Deng, Y.-K. Sun, and K. Amine, Chemistry of Materials **23**, 1954 (2011).
[26] Y. K. Sun, S. T. Myung, B. C. Park, J. Prakash, I. Belharouak, and K. Amine, Nat Mater **8**, 320 (2009).
[27] F. Yang, Science China Physics, Mechanics & Astronomy **55**, 955 (2012).
[28] Y. Li, K. Zhang, and B. Zheng, Journal of the Electrochemical Society **162**, A223 (2014).
[29] Z. Cui, F. Gao, and J. Qu, Journal of the Mechanics and Physics of Solids **60**, 1280 (2012).
[30] J. Crank, *The mathematics of diffusion* (Clarendon Press, 1956).
[31] P. Stein, Y. Zhao, and B. X. Xu, Journal of Power Sources **332**, 154 (2016).
[32] Y. Li, K. Zhang, and B. Zheng, Solid State Ionics **283**, 103 (2015).
[33] K. Zhang, Y. Li, and B. Zheng, Journal of Applied Physics **118**, 175 (2015).
[34] Y. Z. Peng, K. Zhang, B. L. Zheng, and Y. Li, Acta Physica Sinica **65** (2016).
[35] J. W. Choi, J. Mcdonough, S. Jeong, J. S. Yoo, C. K. Chan, and Y. Cui, Nano Letters **10**, 1409 (2010).